12 Nano Metal Particles for Biomedical Applications

Kyung A. Kang, Bin Hong and Hanzhu Jin

Department of Chemical Engineering, University of Louisville
Louisville, KY 40292, USA

Abstract In the management of human health, nano-sized tools are usually more effective than larger ones because they can be incorporated into the systems more in a fundamental (cellular or molecular) level, causing less negative side effects. One of these nano tools that are currently getting much attention is nanometal particle (NMPs). NMPs have many unique properties that are not present in their bulk form. When these unique properties are positively utilized in biological systems they can be very effective for the diagnosis and/or treatment for various diseases. In this article, examples of various applications of NMPs in biomedical sciences and technology are reviewed and a few examples that are currently studied in our research group are demonstrated. It should be noted that, in this article, only a limited publications are cited out of the large volume of NMP related ones, and the readers should not assume that the examples listed in this article are representing all of the currently available NMP tools used in biomedical field. It should also be noted that the authors for this articles are not experts in nanotechnology but are bioengineers.

Keyword Nanometal particles, biosensing, bioimaging, diagnosis, treatment

12.1 NMPs as Contrast Agents for Bioimaging

Many disease diagnoses are done by a principle similar of 'systems identification method,' which has been extensively used for engineering systems for decades. The only difference is that the system, in this case, is a living system. An input signal is applied to, and disturbs the system of our interest, and its responses to the disturbance (i.e. output) is analyzed to understand the system's behavior. For biomedical application, it is highly desirable if the input signal application and the output signal retrieval can be done non- or minimally- invasively. Examples of these inputs for biomedical applications are lights (e.g., ultraviclet (UV), visible, near infrared, and infrared), ultrasound (e.g. sonogram), X-ray (e.g. mammography

(1) Corresponding e-mail: kakang01@louisville.edu

and computerized tomography (CT) scan), electromagnetic wave (e.g. magnetic reasorance spectroscopy (MRS) and magnetic reasonance image (MRI), positron (e.g., positron emission tomography (PET)), etc. The response (output) signal usually provides considerable information about the system but if it is not strong enough then early and/or accurate diagnosis is difficult. Contrast agents that can enhance the signal from the system can, therefore, be very useful especially for this type of situations.

Utilizing NMPs for enhancing the signal from the targeted living system has been attempted in various bio-tools. For MRI, magnetic NMPs are used for this purpose (Weissleder et al., 1990). Superparamagnetic, iron oxides (Fe_2O_3/Fe_3O_4; Feridex I.V.® or Endorem®; Advanced Magnetics, Cambridge, MA) are a few examples of currently used MRI contrast agents. When the surfac of these particles is treated with disease representing biomolecules (e.g. cancer cell specific hormones, antibodies, etc.), the particles can be accumulated much more specifically in the diseased areas, enhancing the contrast for the target and minimizing the negative effect of the particle accumulation in excrtory organs (Josephson et al., 1999; Leuschner et al., 2005).

Nanogold paricles (NGPs) have been extensively used as contrast agents for various imaging techniques. Gold colloids were observed by electron microscopy (Kraemer, 1942) and bio-molecules linked gold colloids were used as targeted contrast agent for this tool. NGPs are also excellent optical contrast agent and, with their inert nature, they can be used for cell and animal studies with less negative side effects than other metals. Figure 12.1(a) shows the optical contrast

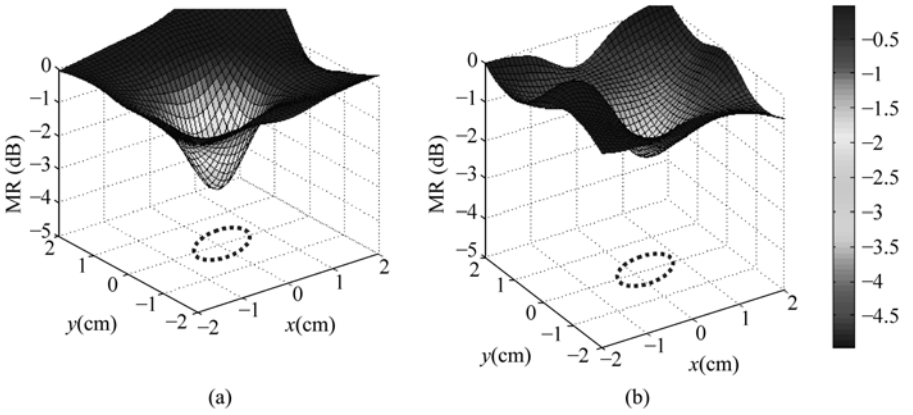

Figure 12.1 Optical contrasts created by an empty vitamin E capsules (oval shape with a dimension of 1.0 cm × 1.0 cm × 1.5 cm) filled with (a) 0.1wt% of 150 nm NGP and (b) 0.1wt% of 10 nm – 20 nm Fe_3O_4 particles, placed 1 cm deep in an experimental breast model whose optical property was adjusted to those of human breast tissue. Near infrared-time resolved spectroscopy (NIR-TRS) spectra, at the wavelength of 788 nm were obtained in transmittance and the spectra were transferred to frequency domain. The modulation frequency analyzed here is at 100 MHz. The black dashed ellipsoids indicate the tumor model size and position (Color Fig. 17)

generated by NGP particles for a near infrared (NIR) wavelength at 780 nm (Jin and Kang, 2007). An empty vitamin E capsule (1.0 cm× 1.0 cm× 1.5 cm) was filled with 0.01wt% NGPs (with the ingredient used for breast tissue model) and placed in an experimental model with the optical properties of human breast tissue. NGPs at a size of 150 nm generate significant optical contrast at a concentration as little as 0.01wt%. Optical contrast generated by Fe_3O_4 particles (10 – 20 nm for this study), which is usually used for MRI contrast and also used for cancer hyperthermia, was also tested for their optical contrast, and they were found to provide a very good optical contrast, although not as strong as NGPs. Loo et al. (2004, 2005) synthesized gold nanoshells filled with silica, which can control optical properties (absorption and scattering coefficients) of the target by the core/shell ratio and the overall size. These particles were conjugated with anti-cancer-antibody and tested for optical, molecular imaging and optical coherence tomography (OCT). With 10 nm gold nanoshells on 120 nm silica core, cancer cells were shown with a significantly increased scattering contrast.

12.2 Fluorescing NMPs

Approximately 50 years ago, Lawson et al. (1960) discovered that, when PbTe and PbSe were evaporated and formed small crystals, photoconductive layers were formed. Later, other researchers (Bergstresser and Cohen, 1967) also found that other semiconductor nanostructures showed excellent fluorescence (Larson et al., 2003). These nano-structures were later named as quantum dots (QDs). Exemplary materials showing these properties in a nano crystal form are CdTe, CdSe, ZnS, and ZnTe. Compared to fluorephores, QDs have advantages of higher quantum yield (QY) and better photo-stability. Since the excitation/emission wavelengths of QDs can be flexibly adjusted either by the size or composition, they can be used for multicolor labeling (Gao et al., 2004) for various biomarkers, which is highly beneficial for multi-biomarker sensing/imanging (Smith et al., 2006).

Recently, QDs has been extensively used for cellular and/or animal studies, although not extensively for human yet. QDs have been very useful for tracking cells and for studying vascular structures (Stroh et al., 2005) and imaging of normal and cancer cells (Kaul et al., 2003); peptide coated, ZnS-capped CdSe QDs showed their accumulating in the lung of mice after the intra venous injection, whereas two other peptide conjugated QDs were directed to blood vessels or lymphatic vessels in tumors (Akerman et al., 2002); Hama et al., (2006) used QDs of two different emission spectra for lymphatic imaging, by the two different size of the QDs. The QDs allowed simultaneous visualization of two separate, lymphatic flow drainages; Stroh et al., (2005) showed that QDs can be used for image and differentiating tumor vessels from the perivascular cells and the matrix. They also used QDs to study the effect of the particle size on the accessibility to

the tumor. QD-labeled, bone marrow-derived precursor cells to the tumor vasculature were successfully monitored; QDs for near infrared (NIR) have been used during a major cancer surgery for mapping sentinel lymph nodes mapping as image guidance. Injection of only 400 pmol of NIR QDs permitted sentinel lymph nodes positioned 1 cm deep to be imaged easily in real time, using excitation fluence rates of only 5 mW/cm^2. Kim et al., (2004), Soltesz et al., (2005), and Gao et al., (2004), reported QD probes for tumor targeting and imaging in live animals. The surface of QDs was treated with the amphiphilic, triblock-copolymer, which then was linked to prostate tumor-targeting antibodies. The study results indicated that the QD probes can be accumulated at human prostate cancer sites in mice by both enhanced permeation and retention, and via the antibody against cancer-specific cell-surface biomarkers. Multicolor fluorescence imaging of cancer cells was achieved under in vivo conditions.

The biocompatibility and the safety of QDs for human use are still under investigation.

12.3 NMPs with High Plamon Field for Fluorescence Manipulation

Fluorephores have a unique property of absorbing a particular wavelength of light and emitting light at another wavelength. For decades, they have been extensively used as effective signal mediators for observing biological phenomena, especially disease related ones, via optical biosensing and bioimaging. As a signal mediator, a fluorophore emitting stronger fluorescence per molecule (i.e. per biomarker) provides a more sensitive tool. This effectiveness gage of a fluorephore is often expressed in terms of its quantum yield, which is the ratio of the number of photons generated for emission to the number of the photons absorbed by a fluorophore.

Many fluorophores have a molecular structure such that their excited electrons are often paired with lone pair electrons within their own molecular structure, without being used for fluorescence emission, which is often called ‘self quenching’ of fluorescence. A strong plasmon field on the surface of a certain type of NMPs can attract these lone pair electrons and alter their fluorescence emission. Good candidate metals possessing a strong plasmon field at their nano-size are gold, silver, and platinum, because of their special molecular nature of holding high electron density around them (Kang and Hong, 2006).

One of the mechanisms of altering fluorescence by these NMPs is as follows: when oscillating electrons in the surface plamon field of an NMP couple with excited electrons of a fluorophore, an instantaneous electron attraction or even an electron transfer occurs from the fluorophore to the NMP, causing the electrons involved in the fluorescence emission altered in their energy states. The level of this alteration depends upon the strength of the plasmon field where the fluorophore is placed. The plasmon field strength depends upon the metal type,

the size of an NMP, from the distance and the nanoparticle (Ruppin, 1975; Geddes et al., 2003; Kang and Hong, 2006; Hong and Kong, 2006).

Placing a fluorophore (or light emitting entities in general, including QDs) around an NMP with high surface plasmon polariton field (SPPF) will result one of the following three scenarios (Fig. 12.2): (a) if the fluorophore is placed very close to the NMP and therefore, is inside an SPPF with a very high strength, then most electrons including the ones for fluorescence emission are attract to the NMP, resulting partial or total fluorescence quenching; (b) If the fluorophore is placed far away from the NMP (outside the plamson field), then there will be little change in the fluorescence; (c) if the fluorophore is at a particular distance from an NMP, where only the electrons that are normally participated in self-quenching are attracted to the SPPF, then the fluorescence is enhanced. In our studies, the spacing between a fluorophore and an NMP was artificially changed by immobilizing self assembled monolayer (SAM) on the surface of NMPs. To avoid the crowding fluorophores, which may result in inter-molecular quecheing, the fluorophore concentration to be tested was very carefully selected, after numerous tests, at the level much lower than the lower limit for this type of quenching.

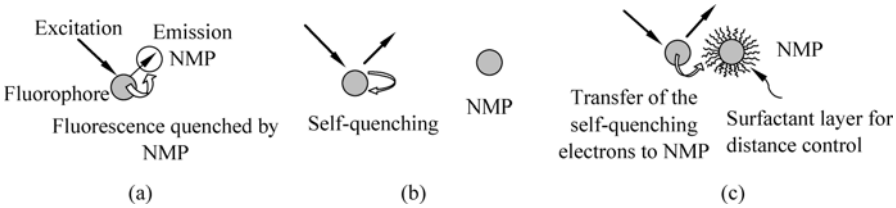

Figure 12.2 A schematic diagram illustrating the effect of the distance between a fluorophore and a nanogold particle on fluorescence: (a) too close—a fluorophore receives excitation light but the emission light is quenched, because the NGP attracts most of the electrons including the ones for fluorescence generation. (b) Too far—the plasmon field around the NGP does not reach the fluorophore. (c) At an appropriate distance—a fluorophore receives the excitation light and an NGP attracts the electrons normally used for self-quenching, resulting in more emission light

The mechanism of quenching and enhancing the fluorescence can be beneficially used, depending upon the specific needs.

12.3.1 NMPs Used for Fluorescence Quenching

As the way fluorescing is used as signal mediation of a biological reaction, quenching can also be used by turning off a steadily-on, fluorescing light or vice versa. Dubertret and his coworkers (2001) have used 1.5 nm nanogold particles to quench fluorescence of fluorephores by attaching an NGP to a single stranded, hairpin DNA (Fig. 12.3). When the probe encounters the target molecule, it forms

a hybrid that is more stable than the hairpin. Then the NGP no longer quench the fluorescence of the fluorophore and fluorescence emit the light; In a slightly different application, Chang and his co-workers (2005) developed a QD with inherent signal amplification upon interaction with a targeted proteolytic enzyme, which is useful for imaging in much better target-specific cancer detection and diagnosis. In this system, QDs are bound to nanogold particles (NGPs) via a proteolytically (collagenase) degradable peptide sequence to suppress luminescence (Fig. 12.4). With the conjugation of NGPs to QDs, 71% reduction in luminescence was achieved. Release of NGPs by peptide cleavage restores radiative QD photoluminescence and, a 52% rise in luminescence over 47 h of exposure to 0.2 mg/mL collagenase.

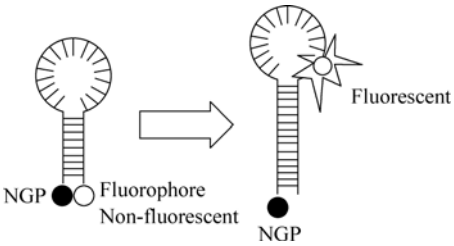

Figure 12.3 An illustration of an NGP quenching fluorescence at a close distance from a fluorophore in a hairpin shaped structure. A target molecule having stronger attraction to the fluorophore than the bond of the hairpin releases the fluorophore from the structure. Then the fluorescence is retrieved

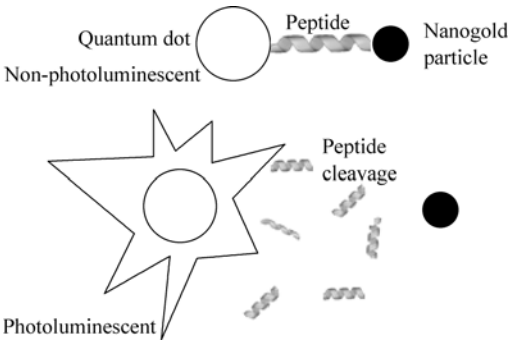

Figure 12.4 A schematic illustration of an NGP's quenching of flurescence of a QD. A protease representing the targeted disease digests the peptide which links the QD and the NGP. As the QD releases it emits intensive fluorescence

12.3.2 NMP for Fluorescence Enhancement in Biosensing

For the fluorescence enhancement by NMPs, here, our study results from the free form of fluorophores in solution (Fig. 12.5(a)) and from a fluorophore mediated,

immuno-biosensing (Fig. 12.5(b)) are illustrated. The basic mechanism of this sensing system is an immuno-sandwich assay on the surface of an optical fiber. Briefly, one type of antibody 1° Mab, specific to the target molecule, is immobilized on the surface of an optical fiber and the fiber is incased in a chamber, forming an immuno-optical sensing unit. The sample is injected to the sensing chamber and the target molecule reacts with the antibody on the fiber surface. The sensor is then washed to remove the non-reacted molecules and another type of antibody linked with a fluorophore –2° Mab is applied to the chamber, to forma sandwich complex. Excitation light is applied to the sensor and then the emitted light is retrieved and correlated to the concentration of the target molecules in the sample. This tool is faster to complete the assay and more user friendly than enzyme linked immuno sorption assay (ELISA). The assay procedure is simpler and can be completed within minutes instead of hours, with the sensitivity as high as a pico molar level. In this article, only the qualitative experimental results are shown and more thorough, quantitative study is currently in progress.

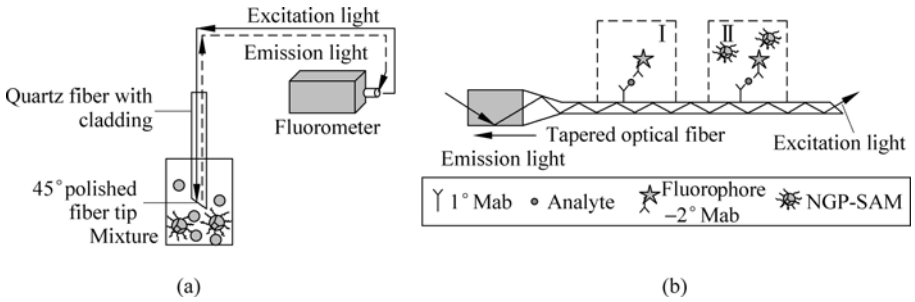

Figure 12.5 Schematic diagrams of fluorescence measurements for (a) free fluorophore and (b) the fluorophore mediated, fiber-optic biosensing

Our definition of enhancement in this study is the increase in the fluorescence divided by the fluorescence intensity without the enhancer (control).

As previously stated, an effectiveness of fluorescence enhancement by an NMP depends upon the strength of SPPF where the fluophore is placed and the SPPF strength around an NMP depends upon the metal type, the size of the NMP, and the distance from the NMP surface. The amount of the fluorescence that can be enhanced by NMPs is that of the normally self-quenched and, therefore, the maximum fluorescence that can be recovered is 1-QY.

To verify this mechanism of the instantaneous transfer of the lone pair electrons from the fluorophore to the NGP, we have performed a simple experiment using pyrrolidine and a fluorophore, Cy5. Pyrrolidine is a small, non-fluorescent molecule with the structure similar to a part of Cy5, which has the nitrogen atom with lone pair electrons. Figure 12.6 illustrates the structures of Cy5 and pyrrolidine, and also their possible interaction with an NGP. According to our theory, Cy5 self-quenches

fluorescence by the intra molecular electron transfer (white ribbon arrow in the figure); Cy5 interacts with the SPPF of an NGP via INTER-molecular electron transfer, resulting in fluorescence enhancement (grey ribbon arrow); added pyrrolidine molecules compete with Cy5 for the interaction with the NGP (black ribbon arrow). Pyrrolidine does not fluoresce, has little steric hindrance because of its small size and therefore, if it is mixed in a solution with Cy5 and NGPs, it can react with NGPs more easyly than Cy5 can. Also, a small amount of pyrrolidine in the solution is not expected to affect chemical or physical properties of the solution (e.g. viscosity, polarity, hydrogen-bonding, etc.). For the experiment, first, Cy5 was dissolved in PBS buffer solution and 5 nm NGP (5 nm NGP) linked with 2 nm self assembled monolayer (SAM) (SAM 2 nm) were added at a molar ratio of Cy5 to NGP, 200∶1 and the fluorescence was measured. At this ratio, approximately 30% of fluorescence enhancement was observed (the initial fluorescence level; Fig. 12.7). Then, pyrrolidine was added to the solution little by little and the fluorescence started to decreased until it reached the fluorescence level of the Cy5 solution without NGPs (dotted line), confirming that NGPs, in fact, interact with the lone pair electrons of Cy5 molecules and cause the fluorescence enhancement.

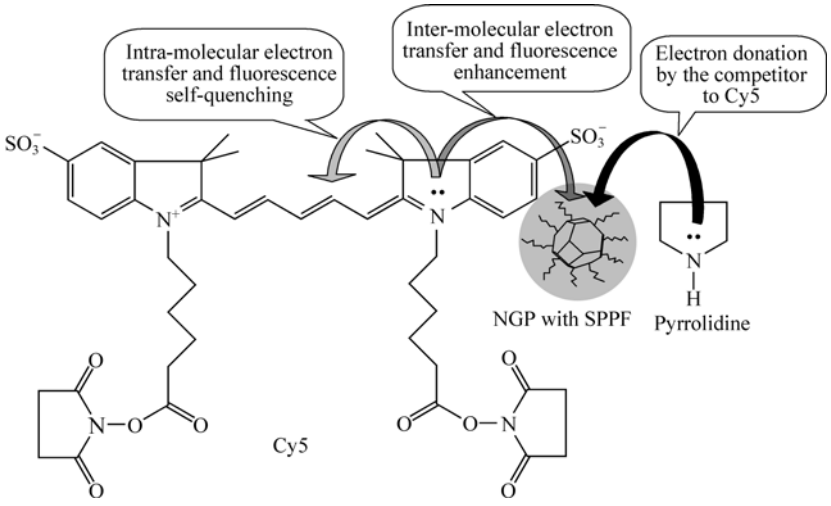

Figure 12.6 A schematic diagram of the interaction among Cy5, pyrrolidine, and an NGP. The white ribbon arrow donates the INTRA molecular electron transfer inside the Cy5. The grey ribbon arrow means the INTER molecular electron transfer between the Cy5 and the NGP. The black ribbon arrow shows the INTER molecular electron transfer between the pyrrolidine and the NGP. Lone pair electrons are shown as double black dots

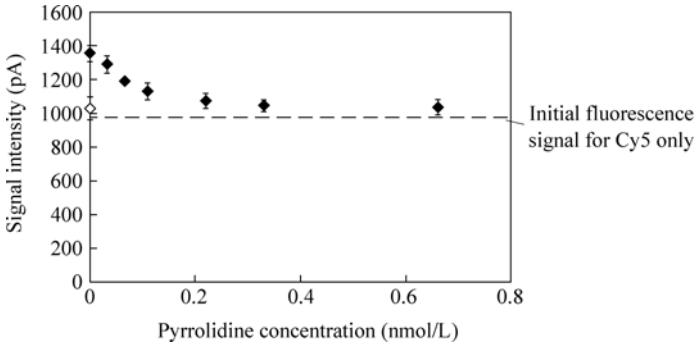

Figure 12.7 The effect of pyrrolidine concentration on the fluorescence enhancement of free Cy5 by NGPs. The signal intensity of Cy5 solution without NGPs was shown as the dotted line (Experimental conditions: Free Cy5 concentration, 66 nmol/L; 5 nm NGP-SAM 2 nm concentration, 0.33 nmol/L)

1. Metal Type

For this part of study, nanosilver particles (NSPs) and NGPs at a size of 20 nm were selected. 20 nm was chosen simply because, at the time of our study, it was the smallest size that was commercially available for NSP. These nanoparticles are sold with tannic acid (length, ~3 nm) as surfactant (SAM 3 nm) on their surface. These particles were tested in fluorophore mediated, sandwich immuno-sensing of a cardiac marker B-type natriuretic peptide (BNP) in human plasma at a concentration of 0.5 ng-BNP/mL-plasma (Fig. 12.8), while the nanoparticles are applied after the sandwich complex is formed on the senor surface (Fig. 12.5(b)). In this study, the particle concentration was set to be 0.2 nmol/L since it was the optimal NGP concentration with our biosensor studies. As can be seen in Fig. 12.8, NSPs showed the enhancement of 30%, and NGPs, 114%, illustrating the differences in plasmon strength for different metals.

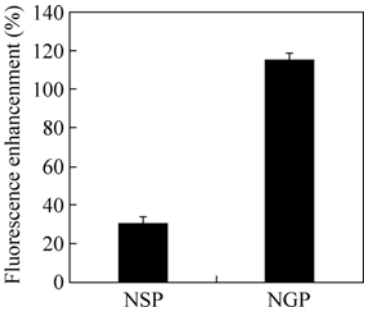

Figure 12.8 Fluorescence enhancement in BNP biosensing by 20 nm NSP-SAM 3 nm and 20 nm NGP-SAM 3 nm (Experimental conditions: fluorophore used, Cy5; sensor size, 1.5 cm; BNP concentration, 0.5 ng-BNP/mL-plasma, NGP-SAM concentration, 0.2 nmol/L)

2. Particle Size

The effect of the NMP size was studied using the NGPs at sizes of 2, 5, and 10 nm (commercially available ones). For this study, the thickness of a SAM remained to be 3 nm (SAM 3 nm; tannic acid). The measurement on the emitted fluorescence was both for a free Cy5 and for immuno-biosensing Fig. 12.9. The enhancement for the free Cy5 by 2, 5 and 10 nm NGPs were 42%, 30%, and 11%, respectively, showing a less enhancement with the greater NGP size, confirming the differences in the plasmon density for the NGPs at different sizes. For the biosensing, protein C (an anticoatulant in plasma) was used an analyte and, the enhancements were 115%, 102%, and 12%, respectively. There were similar trend in the enhancement for free Cy5 or Cy5 mediated sensors qualitatively, but the biosensing showed much higher enhancment. This may be because free fluorophores suspended in solution interact with the NGPs in a three-dimensional space, while the biosensing provides the surface-bound fluorophores, and therefore, the fluorescence retrieval is much more effective.

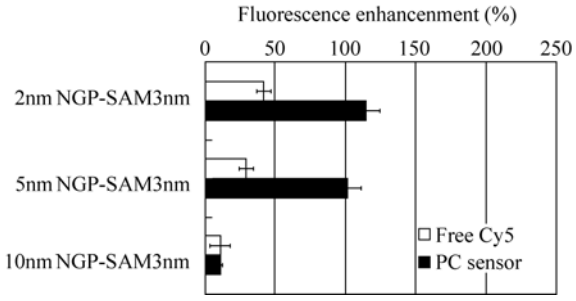

Figure 12.9 The effect of the NGP size on the fluorescence enhancement for the free Cy5 and the Cy5 mediated PC sensing (Experimental conditions: For free Cy5 measurement, the concentration of Cy5, 66 nmol/L; PC sensor size, 6 cm; PC sample, 1 μg-PC/mL-plasma; SAM thickness, 3 nm; NGP size used, 2, 5, and 10 nm)

3. Distance between a Fluorophore and an NMP

As previous stated, here, the spacing between a fluorophore and an NMP was artificially changed by immobilizing self assembled monolayer on the surface of NMPs. However, the SAM thickness here is not the actual distance but the minimum distance between a fluophore and an NGP because NGPs are floating in a solution. The SAMs at approximately 1, 2, and 3 nm (*L*-glutathione, 16-mercaptohexadecanoic acid, and tannic acid, respectively) were reacted with NGPs at a size of 5 nm (5 nm NGP). The 5 nm NGPs coated with SAMs (5 nm NGP-SAMs) were then applied to both the free Cy5 and the Cy5 mediated PC biosensor, and the level of enhancement was observed (Fig. 12.10). For both the free Cy5 and PC sensors, the SAM thickness of 2 nm (SAM 2 nm) demonstrated

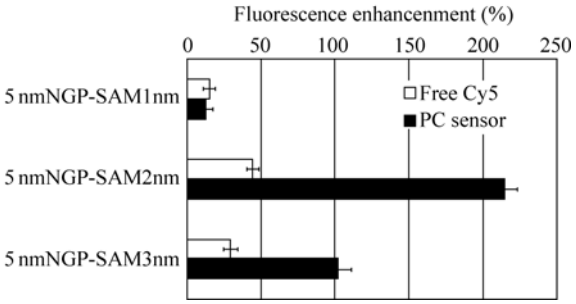

Figure 12.10 The effect of the SAM thickness on the fluorescence enhancement for the free Cy5 and the Cy5 mediated PC sensing (Experimental conditions: for free Cy5 measurement, the concentration of Cy5, 66 nmol/L; PC sensor size, 6 cm; PC as sample)

the greatest enhancements. Although there was enhancement, 1 nm may have been too close to prevent reduction in radiative emission, and 3 nm, too far to reroute the electrons for effective enhancement.

4. Quantum Yield of Fluorophore

As stated, the maximum amount of the enhanced (retrieved) fluorescence depends upon the QY of a fluorophore. In other words, if the quantum yield of a fluorophore is low due to the extensive self quenching, then the amount of fluorescence to be retrieved would be higher. To test this hypothesis, Alexa fluor^{TM} 647, another fluorophore that has very similar maximum excitation and emission (Ex/Em) wavelengths with a QY different from that of Cy5, was selected. The QYs of Cy5 and AF647 are ~0.28 and ~0.56, respectively, and both have the excitation and emission maxima at or around 649 and 670 nm, respectively (Anderson and Nerurkar, 2002; Berlier et al. 2003). As can be seen in Fig. 12.11, for the free fluorophore, AF647 showed only a small enhancement and for the PC biosensing, it showed none, indirectly showing the effect of QY on the enhancement level.

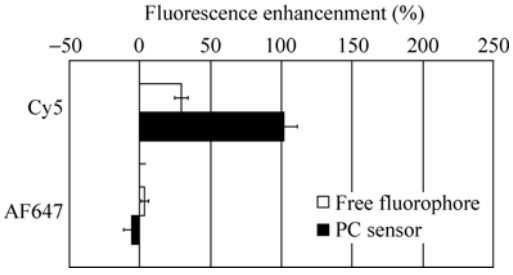

Figure 12.11 The effect of the fluorophore quantum yields on the fluorescence enhancement for the free fluorophore and the fluorophore mediated PC sensing (Experimental conditions: For the measurement of free fluorophores, the concentration of Cy5 and AF647, 66 nmol/L; PC sensor size, 6 cm; NGP-SAM used: 5 nm NGP-SAM 3 nm)

12.3.3 NMP for Fluorescence Enhancement in Bioimaging

When a fluorophore is used for in-vivo bio-imaging, unlike in ex-vivo biosensing or bioimaging, the fluorophore and the NMP may not be separately applied to the system. In bioimaging, fluorophores are usually designed to target specific bio-molecules in the cell or organelle and if these two entities are separately applied there is no guarantee that both would arrive together at the target site, although special manipulation may be designed to do so. Therefore, the fluorophore needs to be somehow immobilized to the NMP with a spacer appropriate for the enhancement. Indocyanine green (ICG; Cardio-green) is an FDA approved NIR contrast agent but a rather poor fluorophore, in terms of the quantum yield (QY = 0.032 in plasma; Licha et al., 2000). Maximal excietation and emission wavelengths for ICG are 780 and 830 nm, respectively. Since ICG does not have any side chain to react, Cypate, an ICG derivative with a carboxylic group was used (Achilefu et al., 2000). For this study, commercially available protein A (PA: 1 nm) or streptavidin (SA: 3 nm) linked 5 or 10 nm NGPs were used. Since multiple numbers of these protein molecules are immobilized on the surface of an NGP the resulting Cypate linked NGPs via these proteins would probably be as shown in Fig. 12.12. Cypate was linked to 5 or 10 nm NGP-PA and NPG-SA

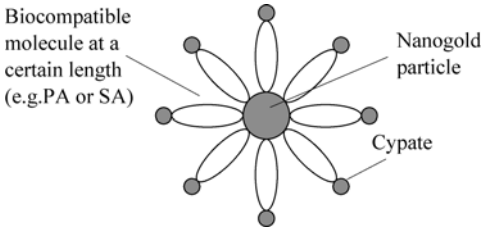

Figure 12.12 A schematic diagram of possible binding struture of Cypate and NGP via protein A (PA) and stepavidin (SA)

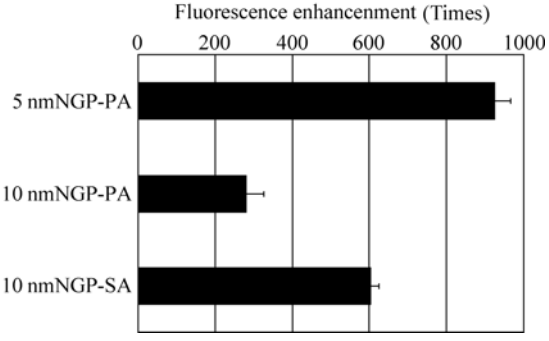

Figure 12.13 Fluorescence enhancement by Cypate linked, PA coated, 5 nm NGP (5 nm NGP-PA), PA coated 10 nm NGP (10 nm NGP-PA), or SA coated 10 nm NGP (10 nm NGP-SA) compared to Cypate alone (Experimental conditions: Cypate concentration, 30 μmol/L)

and the resulting fluorescence of Cypate-PA/SA-NGP was compared to that of Cypate only (Fig. 12.13). The fluorescence signal by Cypate linked 5 nm NGP, via PA spacer showed the best performance and the enhancement level was as high as 900 times. For the 10 nm NGP, 3 nm-spacer (SA) provided a higher enhancement than 1 nm-spacer (PA). This result shows that NMPs (in this case NGPs) with high biocompatibility, can be highly effective for enhancing the fluorescence of the fluorophores that can be used for bio-imaging of human.

12.4 Magnetic NMPs for Bioseparation

The size of the magnetic particles for bio-separation application is usually larger than the usual sense of 'nano' (equal or less than 100 nm), because the particle needs to be big enough to generate sufficient magnetic force, to be effective for the separation purpose. These particles are usually surface treated with anti-target molecules. The anti-target molecule on the surface of the particles reacts with the target molecule and the target molecule containing magnetic particles are then captured by a magnetic field or a type of particle separating systems. After the particles are washed to remove un-wanted/un-reacted materials from the surface and then the target molecule can be retrieved by releasing them from the anti-target molecule by changing the liquid condition where the particles are placed. After removing the target molecules, the particles can be used again. Here we are listing some of the application examples.

Coker et al. (1997) have used polyacrylamide/magnetite (PAM) composite beads in a magnetically stabilized fluidized bed (MSFB). The PAM beads were stable in most buffers from pH 1.1 to 10. This approach allowed MSFB operation at superficial velocities close to those used in high pressure liquid chromatography (HPLC) (~0.1 mm/s) with a magnetic field applied to stabilize the bed. The beads were used in affinity separation of chymotrypsin from the sample of a mixture with equal concentrations of trypsin and chymotrypsin. Although the adsorption capacity of the beads was less than that of other beads the purity of the product was higher; Magnetic agarose beads were used to separate angioI-TEM-ρ-lactamase from *E. coli* lysate and able to concentrate the target molecule without a centrifugation process (Abudabi and Beitle 1998). This method is especially good for separating biomolecules in a highly viscous fermentation broth with various lysates because particles in such a broth are not easily centrifuged, filtered, or separated by packed bed chromatography; Yang and his colleagues (2006) used magnetic poly methyl methacrylate (PMMA) beads coated with polyethylene glycol and functionalized with amine groups. *P*-aminobenzamidine was covalently immobilized onto magnetic beads for the purification of nattokinase directly from the purification broth. The purification process took only 40 minutes with a purifcation factor of 8.76 and a yield of 87%; Magnetic adsorbent (i.e.

ferro-carbon particle) has been used to adsorb toxic materials at low, medium and high molecular weights from blood stream (Torchilin and European 2000). A high gradient magnetic separator is used to remove the tonxin adsorbed, magnetic particles from the blood stream. Animal experiments have shown high effectiveness of the removal of low molecular weight toxins using this technique.

12.5 Magnetic NMPs for Biosensing

Most sensing techniques separate the target molecule from the mixture with other molecules in the sample, before the actual application of a signal mediator for sensing. As shown in the previous section, magnetic force can also be used for separating the target molecule utilizing anti-biomarker conjugated nano- (or micro-) sized superparamagnetic particles. For sensing, the target molecule bound on the particle surface is quantified by several different way: for examples, the change in the interference in magnetic field due to the particles, the chemical signal created by the reaction between the target molecule on the particle surface and another molecule that develops color, the change in the magnetic field strength by the magnetic particles reacted with the anti-target molecules, etc. Figs. 12.14 and 12.15 illustrate one of the elegantly designed sensing techniques using magnetic particles, which was developed by the Dr. C. H. Ahn research group at the University of Cincinnati (with the permission of Dr. Ahn; Choi et al., 2002). Figure 12.14 illustrates the procedure for their immunoassay using magnetic particles with a chemical detection system: First, magnetic beads coated with

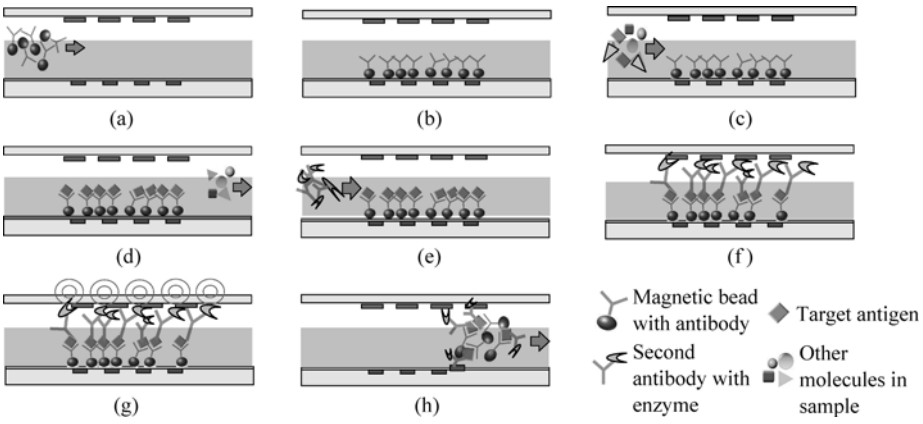

Figure 12.14 Schematic diagrams of the immunoassay using magnetic particles: (a) injection of magnetic beads conjugated with antibody to the chamber. (b) separation and holding of beads. (c) introduction of samples. (d) immuno-reaction with the target antigen. (e) second antibody application. (f) excess second antibody is washed away. (g) antigen sensing. (h) regeneration of the sensor (Provided by Dr. C. H. Chong at the University of Cincinnati)

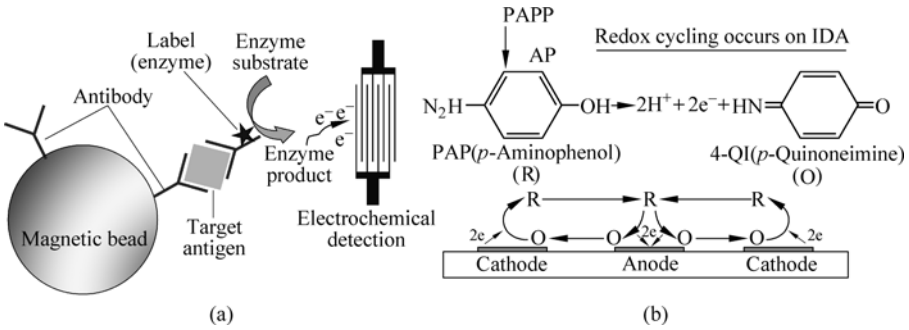

Figure 12.15 Schematic diagrams of the immunoassay with detection by electrochemistry: (a) magnetic particle-based immunoreaction and detection and (b) redox cycle electrochemical sensor combined with immunoreaction (Provided by Dr. C. H. Chong at the University of Cincinnati)

antibodies are injected into the sensing chamber and beads in the chamber are held by magnetic force on the wall of the sensing chamber. When the sample is introduced to the chamber, immunoreaction occurs between the antibody on the particle surface and the target antigen. After the magnetic particles are washed to remove unreacted biomolecules, the second antibody is applied and the antigen on the particle reacts with the second antibody. After this reacrtion, the excess antibody is washed away and the amount of antigen is quantified by an enzymatic reaction (Fig. 12.15(a)) between the second antibody and another molecules generating chemicals that can be quantified by electro- chemical sensing (Fig. 12.15(b)). After the assay, the magnetic field is removed and the particles are washed away and the sensing system is ready for a new assay, enabling continuous sensing.

Many other researchers have also used magnetic particles for sensing. Meyer, and his co-workers used magnetic beads labeled with antibodies against a cardiac marker c-reactive protein and pathogenic bacteria (Meyer et al., 2007a, 2007b, 2007c; in press-b), at a highly sensitive level. The mechanism of sensing is as follows: An immuno affinity chromatography column captures the target molecule in the sample and then magnetic particles coated with another type of antibody are run through the column. The antibodies on the surface of magnetic particle are captured by the target molecule in the column. When the magnetic force at a certain frequency is applied to the column, then the response from the column changes with the level of captured magnetic particles. By correlating this change and the concentration of the anlayte in the sample, they were able to accurately quantify/detect the target molecules in the sample; Bulte and his co-workers (1999, 2001) used 'magnetodendrimers' to track cell migration and myelination and also to track the stem cell migration; Varshney and Li (2007) have developed an impedance biosensor based on the integrated arrayed microelectrode coupled with magnetic nanoparticle–antibody conjugates, to detect *E. coli* in ground beef; Lermo, et al. (2007) used magnetic beads for DNA amplification directly with a

novel magnetic primer. Their DNA biosensor was able to detect the changes at single nucleotide polymorphism level, when stringent hybridization conditions were used. The sensor was tested for *Salmonella spp*.; Gorschlüeter et al. (2002a; 2002b) developed analyte-labeled magnetic microparticles. Detection is achieved by measuring electrochemical current changes occurring when bead-labeled analyte molecules get specifically bound to microelectrodes. When the magnetic force exceeds the specific binding force of the analyte molecule, the bound microparticles are removed. Then a signal is generated, and a transducer measures the specific binding forces; Graham et al. (2003) used a micron sized sensors to detect the binding of single streptavidin functionalized, 2 μm magnetic microspheres on a biotinylated sensor surface; Connolly and St. Pierre (2001) developed a method based on the detection of shifts in the frequency-dependent magnetic susceptibility of magnetic colloids caused by the increase in hydrodynamic radius by the specific binding of biomolecules.

12.6 Magnetic NMPs for Cancer Hyperthermia

Hyperthermia for cancer treatment can be done either by ablating tumor with a high thermal energy or by applying low heat to keep the diseased tissue at 42 – 45℃. At this temperature the enzymes required for cell survival get deactivated and cells slowly die. The low heat hyperthermia is, therefore, a cancer treatment with a minimal damage to the normal tissue (Storm, 1983). Utilization of magnetic particles for hyperthermic therapy was first investigated by Gilchrist et al. (1957). They injected iron oxide particles into lymph nodes of dogs and observed temperature increases of approximately 5℃ after exposuing the animals to an alternating electro magnetic (AEM) field. Magnetic nanoparticles can be effectively heated in AEM field by hysterisis loss, Neel relaxation, or/and Brownian relaxation (Hergt et al., 1998). When magnetic materials with multi- domains are exposed to a magnetic field, the domain with the same direction of applied magnetic field grows and the other ones shrink. This domain replacement in the material along the AEM field produces heat by hysterisis loss. Neel Relaxation is due to the rotation of the internal magnetic dipole in the single-domain particles along the AEM field. When the carrier liquid for these particles has a sufficiently low viscosity, heat can also be generated by the physical rotation of the particles along the applied AEM field, which is called Brownian Relaxation. When these magnetic NMPs are placed in AEM, depending on the mean particle size and the properties of the medium where they are placed, one or multiple heating mechanisms may be involved (Andra and Nowak 2007; Hergt et al., 2002). One of the most frequently used particles for hyperthermia is Fe_3O_4 nanoparticle (Jordan et al., 1999; Bahadur and Giri 2003; Tartaj et al., 2003; Momet et al., 2004) or Fe_2O_3 particle (Yan et al., 2005). As previously stated, FDA has approved iron oxide based MRI contrast agents for human use.

These nanoparticles are often coated with biocompatible materials. Examples of these materials are dextran (Jozefczak and Skumiel 2007; Zhang et al., 2007), Polyethylene glycol (PEG; Acar et al., 2005; Shultz et al., 2007), liposome (Yanase et al., 1998; Hamaguchi et al., 2003; Matsuoka et al., 2004; Kawai et al., 2005; Tanaka et al., 2005), or other biocompatible polymers (Zhao et al., 2005). The coating makes the particles hydrophilic without immunogenic response when injected in vivo. Hilger et al. (2005) have applied dextran coated Fe_2O_3 and Fe_3O_4 particles at a size range of $10-20$ nm for hyperthermia. After injecting these partides to mice, intra-tumorally (~22 mg-NMP/ 3 cm^3-tumor), by applying AEM at a frequency of 0.4 MHz and the field amplitude of 6.5 kA/m, for four minutes, the temperature at a center of the tumor was raised up to 71℃; Cancer-specific antibodies are also frequently linked to the coated layer for enhancing the tumor targeting ability (Shinkai et al., 2001; Gruttner et al., 2006).

The AEM applicator for hyperthermia can be usually either a coil shape or a pancake shape but for a non-invasive application of AEM to a large organ, the pancake shape may be more accommodating. Also, one can use more than one applicators for applying the AEM field properly to the magnetic particle accumulated, tumor site. Mathematical estimation of AEM field distribution can be helpful for designing an appropriate geometry of applicator(s). An example of simulated, AEM field strength distributions for a single and a double pancake type applicators is shown in Fig. 12.16. The level of brightness shows the density of the magnetic field. For the single pancake-shaped applicator, the field density seems to be distributed close to the surface of the applicator, with only a little depth penetration (Fig. 12.14(a)). For the two-pancake system with the same current flow directions for both, the magnetic density between two applicators are greatly enhanced, also increasing the penetration depth (Fig. 12.16(b)).

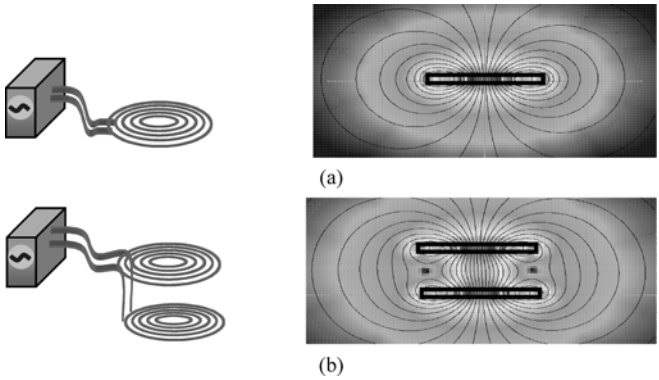

Figure 12.16 Schematic diagrams of (a) a single and (b) a double pancake-shaped AEM applicators and the simulation result of the magnetic field distribution (front view)

The AEM frequency at a giga hertz level is the microwave that we is used at home and at this frequency, dielectric heating occurs, which should be avoid in magnetic nanoparticle mediated hyperthermia. We have performed a study to select the proper AEM frequency range that can heat nanoparticles, without heating normal tissue (Jin and Kang, 2007). The samples that we tested were distilled water, bovine hemoglobin solution at a concentration of 0.14 g/mL-water (concentration in normal blood), NaCl solution at 0.9% (physiological concentration), and the ground beef. 4 ml of each sample in a glass tube was placed inside the solenoid shaped induction heater coil, at frequencies of 0.45, 5.4, and 9.2 MHz, at 5 kW for 2 minutes. The distilled water was not heated at all three frequencies. Hemoglobin was not heated at the frequencies tested, either. The NaCl solution was heated extensively at 5.4 and 9.2 MHz. The ground beef was also heated at 5.4 and 9.2 MHz, probably due to the salt content in the meat. The frequency of 0.45 MHz was, therefore, selected for the next studies.

The heating performance of various particle sizes was studied at 0.45 MHz and 5 kW (Fig. 12.17). The temperature increases in agar containing Fe_2O_3 or Fe_3O_4 nanoparticles at concentrations from 0.1wt% to 1wt% were measured after 2 min of exposure in a solenoid shaped AEM applicator. For all particles, the heating was linearly proportional to the particle concentration in the sample. For the samples containing Fe_3O_4 at 10 – 20 nm or 20 – 30 nm, the temperature increases were approximately at a rate of 35℃/wt% of particles. With Fe_3O_4 particles at 40 – 60 nm, however, it was 9℃/wt%, indicating that the heating capability of Fe_3O_4 nanoparticles depend on their particle sizes. For the sample containing 20 – 30 nm Fe_2O_3, the rate of temperature increase was 30℃/wt%, which was very close to the Fe_3O_4 particles at the size range of 10 – 30 nm. For the Feridex I.V.® (FDA approved MRI contrast agent) which are a 5 nm Fe_3O_4 particles, the rate of temperature increase was 3℃/wt%, lower than that for other sizes but, with increases in heating time, this slower heating rate can be compensated.

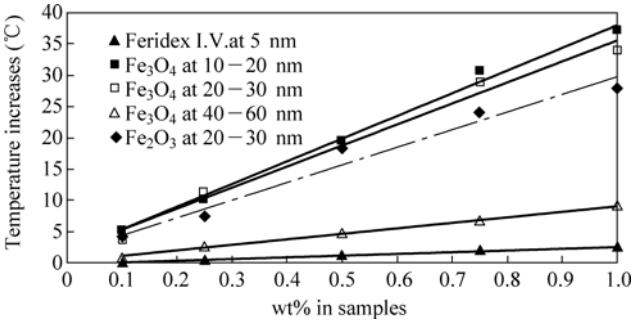

Figure 12.17 The effect of particle size on heating performance of iron oxide nanoparticles by AEM field The concentrations of iron oxide in the samples were 0.1wt% – 1wt%. The samples were heated at a 0.45 MHz frequency and 5 kW power for 2 min

12.7 Multi-Functional NMPs

The most desired method for managing disease is the detection/diagnosis at an earliest possible stage and also the treatment at the same time or immediately after the diagnosis. For this approach, researchers have been developing multifunctional entities with the three important properties—the biomarker targeting, the detection, and the treatment. Also, for each property, one may use multiple modalities for more accuracy. Liposomes (Saito et al., 2004), dendrimers (Majoros et al., 2005), and encapsulation (Reddy et al., 2006) may have been more frequently used methods for this purpose. For NMPs, QDs are starting to be used for this multifunctional approach (Sinha et al., 2006). Also, since many MRI contrast agents are based on Fe_3O_4 particles, researchers manipulate the particle to add more functions to them (Fortina et al., 2007). One good example for this multifunctional appoach is the study results by Dr. Naomi Halas's research group at the University of Rice. They have developed optically tunable nano gold shells filled with dielectric core, functionalized with cancer specific antibodies for cancer targeting. The scattering property of the particle was used for cancer detection and the optical heating was used for cancer therapy (Loo et al., 2005; Fortina et al., 2007).

Here, an example of the development of a multifunctional NMP studied in our research group is illustrated with more details. As shown in our previous study results above, Fe_3O_4 nanoparticles at size 5 – 60 nm are heated well, especially at the range of 10 – 30 nm, in the AEM field at a frequency of 0.45 MHz and a power of 5 kW, without heating any tissue components (see Section 12.6 in this article). Fe_3O_4 nanoparticles are reasonably good near infrared (NIR) absorbers (Fig. 12.1(b)). But NGPs at a size range of 10 – 250 nm are even stronger NIR absorbers (Fig. 12.1(a)). Gold has other advantageous properties, such as, the chemical inertness, the ability of easily conjugating biologicals, and also the property of quenching/enhancing fluorescence (see Section 12.3 in this article). Therefore, gold coated Fe_3O_4 nanoparticles (Jin and Kang, 2007) can act as good NIR absorber and highly effective fluorescent contrast agent with Cypate linkage for optical breast cancer detection (Jin and Kang, 2006), and also thermal guide for tumor hyperthermia. The gold coated Fe_3O_4 particles did not lose its heating capability (Jin and Kang, 2007) and the NIR absorption and also flurorescence enhancing property were excellent. For this particular example, the cancer targeting moiety was luteinizing hormone-releasing hormone (LHRH). Many cancer types including breast cancers express receptors for LHRH and most visceral organs do not express LHRH receptors, or express only at a low level (Kakar, 2003). LHRH is a peptide of 10 amino acids and spontaneously reacts with the surface of nanometal particles by its *N*-terminal amine group via its self-assembling nature. Also, as a cancer targeting agent, LHRH can be much more economical than

humanized monoclonal antibodies. Researchers have demonstrated that the breast cancer cells can be targeted through their high affinity LHRH receptors present on the cell membrane (Leuschner et al., 2005; Kakar et al., 2008). As an initial test for using LHRH as a tumor targeting agent, LHRH was linked to NGPs or Fe_3O_4 nanoparticles (eventually LHRH will be linked to gold-coated Fe_3O_4 nanoparticles) (Fig. 12.18). The binding affinity of LHRH linked NGPs was studied using the mouse gonadotrope cell line (LβT2) expressing LHRH receptors. LHRH-linked NGPs showed a similar binding affinity (about 0.1 nmol/L) to the native LHRH peptide, suggesting that the LHRH conjugated NGP retains its binding affinity (Jin and Kang, 2008).

The ultimate goal of our study is to build a multi-fuctional nanoentity, LHRH and Cypate linked, gold coated Fe_3O_4 nanoparticle. These particle can provide the properties of cancer targeting, high NIR absorption and fluorescence, also possibly providing MRI contrast, for a minimally invasive, early cancer diagnosis, and minimally invasive hyperthermic treatment of cancer (Fig. 12.19).

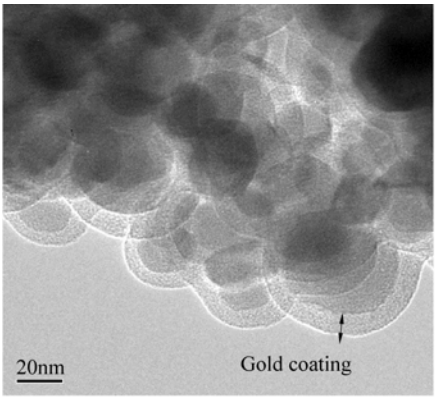

Figure 12.18 A TEM image of gold coated Fe_3O_4 nanoparticles

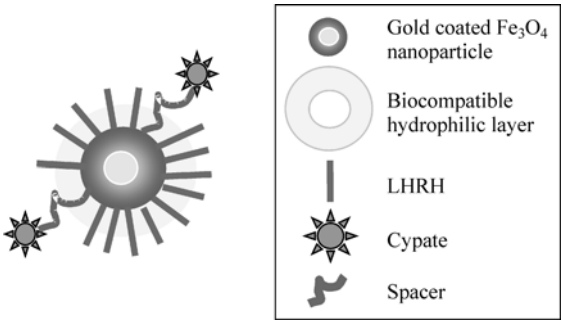

Figure 12.19 A multi-functional nano entity with the properties of cancer targeting, a high absorption/flurescnece/MRI contrasts and cancer hyperthermia by AEM energy

12.8 Conclusions

The biomedical applications of nanometal particles have been expanding rapidly and will be even more popular as time passes because of their numerous advantageous natures in the size and also the unique and beneficial properties of nano-sized metals, as described in the article. It is evident that the examples that are listed in this article are only a small portion of the currently used NMPs for biomedical applications. One task still remained to be seriously studied for the in-vivo application of these particles is the possible toxicity of metal particles in human body and also the accumulation in the excretoray organs. Also the clustering tendency of NMPs due to the unstable nature of nanosized materials needs to be overcome for more general use of these partilces. The active efforts by many multi-disciplinary scientists toward resolving these issues are expected to enable the utilization of NMPs for human being soon.

Acknowledgements

The authors acknowledge the Kentucky Science and Engineering Foundation for the financial support of the metallic nanoparticle study and the National Science Foundation (BES-0330075) for funding on Protein C and the cardiac marker biosensing system. The authors would also like to express thanks to Dr. Achilefu for supplying Cypate for our study. We appreciate Dr. C. H. Ahn at the University of Cincinnati for providing figures for their sensing system using magnetic particles and Dr. Donglu Shi at the University of Cincinnati for providing the gold coated Fe_3O_4 particles and the TEM images.

References

Abudabi, T. and R.R. Beitle, *J. Chromatogr.* A **795**: 211 (1998).

Acar, H., R.S. Garass, F. Syud, P. Bonitatebus and A.M. Kulkarni. *J. Magn. Magn. Mater.* **293**(1): 1 (2005).

Achilefu, S., R.B. Dorshow, J.E. Bugaj, R. Rajagopalan. *Invest Radiol.* **35**: 479 (2000).

Akerman M.E., W.C. Chan, P. Laakkonen, S.N. Bhatia and E. Ruoslahti. *Proc. Natl. Acad. Sci.* USA **99**: 12,617 (2002).

Anderson, G.P. and N.L. Nerurkar. *J. Immunol Methods.* **271**: 17 (2002).

Andra, W. and H. Nowak. *Magnetism in Medicine.* Berlin: Wiley-VCH (2007).

Bahadur, D. and J. Giri. *Sadhana* **28**(3&4): 639 (2003).

Berlier, J.E., A. Rothe, G. Buller, J. Bradford, D.R. Gray, B.J. Filanoski, W.G. Telford, S. Yue, J. Liu, C-Y Cheung, W. Chang, J.D. Hirsch, J.M. Beechem, R.P. Haugland and R.P. Haugland. *Journal of Histochemistry and Cytochemistry* **51**(12): 1699 (2003).

Bulte, J.W.M., S.C. Zhang, P. van Gelderen, V. Herynek, E.K. Jordan and I.D. Duncan. *Proc. Natl. Acad. Sci. USA* **96**(26): 15,256 – 15,261 (1999)

Bulte, W.M.J., T. Douglas, B. Witwer, S-C. Zhang, E. Strable, B.K. Lewis, H. Zywicke, B. Miller, P. van Gelderen, B.M. Moskowitz, I.D. Duncan and J.A. Frank. *Nat. Biotechnol.* **19**: 1141 (2001).

Chang, E., J.S. Miller, J. Sun, W.W. Yu, V.L. Colvin, R. Drezek and J.L. West. *Biochemical and Biophysical Research Communications* **334**(4): 1317 (2005).

Choi, J., K.W. Oh, J.H. Thomas, W.R.Heineman, H.B. Halsall, J.H. Nevin, A.J. Helmicki, H.T. Henderson, C.H. Ahn. *Lab Chip* **2**: 27 (2002).

Cocker, T. M., J.F. Conan and A.E. Rachel. *Biotechnol. Bioeng.* **53**: 79 (1997).

Connolly, J. and T.G. St Pierre. *J. Magn. Magn. Mater.* **225**: 156 (2001).

Dubertret, B., M. Calame, A.J. Libchaber. *Nat. Biotechnol.* **19**: 3659 (2001).

Gao, X.H., Y.Y. Cui, R.M. Levenson, L.W.K. Chung and S.M. Nie. *Nat. Biotechnol.* **22**: 969 (2004).

Geddes, C.D., A. Parfenov, D. Roll, M. J. Uddin, and J. R. Lakowicz. *Journal of Fluorescence* **13**(6): 453 (2003).

Fortina, P., L.J. Kricha, D.J. Graves, J. Park, T. Hyslop, F. Tam, N. Halas, S. Surrey, S.A. Waldman. *Trends Biotechnol.* **25**(4): 145 (2007).

Gilchrist, R.K., R. Medal, W.D. Shorey, R.C. Hanselman, J.C. Parrott and C.B. Taylor. *Ann Surg.* **146**(4): 596 (1957).

Gorschlüter, A., C. Sundermeier, B. Roß and M. Knoll. *Sens. Actuators* B **85**: 158 (2002a).

Gorschlüter, A., L.H. Mak, C. Sundermeier, B. Roß and M. Knoll. *Biomed. Tech.* **47**: 213 (2002b).

Graham, D.L., H.A. Ferreira, P.P. Freitas, and J.M.S. Cabral. *Biosensors and Bioelectronics.* **18**: 483 (2003).

Gruttner, C., K. Muller, J. Teller, F. Westphala, A. Foreman and R. Ivkovb. *J. Magn. Magn. Mater.* **311**: 181 (2007).

Hama, Y., Y. Koyama, Y. Urano, P.L. Choyke and H. Kobayashi. *Breast Cancer Res Treat.* **17**(6): 1426 (2006).

Hamaguchi, S., I. Tohnai, A. Ito, K. Mitsudo, T. Shigetomi, M. Ito, H. Honda, T. Kobayashi and M. Ueda. *Cancer Sci.* **94**(9): 834 (2003).

Harisinghani, M.G., S. Saini, R. Weissleder, P.F. Hanh, R.K. Yantiss, C. Tempany, B.J. Wood and P.R. Mueller. *Am. J. Roentgenol.* **172**: 1347 (1999).

Hergt, R., W. Andra, C.G. d'Ambly, I. Hilger, W.A. Kaiser, U. Richter, and H. Schmidt. *IEEE Trans. Magn.* **34**(5): 3745 (1998).

Hergt, R., R. Hiergeist, I. Hilger and W.A. Kaiser. *Recent Res. Dev. Mater. Sci.* **3**: 723 (2002).

Hilger, I., R. Hergt and W.A. Kaiser. *J. Magn. Magn. Mater.* **293**: 314 (2005).

Hirsch L.R., R.J. Stafford, J.A. Bankson, S.R. Sershen, B. Rivera, R.E. Price, J.D., Hazle, N.J., Halas, J.L. West. *Proc. Natl. Acad. Sci.* USA **100**(23): 13,549 (2003).

Hong, B. and K.A. Kang. *Biosensor and Bioelectronics* **21**: 1333 (2006).

Inoue, S., M. Goda, H. Du, M.D. Disney, B.L. Miller and T.D. Krauss. *Biol. Bull.* **201**: 231 (2001).

Jin, H. and K.A. Kang. *Advances in Experimental Medicine and Biology* **566**: 167 (2005).

Jin, H. and K.A. Kang. *Advances in Experimental Medicine and Biology*, **599**: 45 (2007).

Jin, H, B. Hong, S.S. Kakar and K.A. Kang. *Advances in Experimental Medicine and Biology*, **614**: 275 (2008).

Jozefczak, A. and A. Skumiel. *J. Magn. Magn. Mater.* **311**(1): 193 (2007).

Jordan, A., R. Scholz, P. Wust, H. Fahling and R. Felix. *J. Magn. Magn. Mater.* **201**: 413 (1999).

Josephson, L., C.H., Tung, A. Moore, R. Weissleder. *Bioconjuate Chem.* **10**: 186 (1999).

Kakar, S.S., S.J. Winters, W. Zacharias, D.M. Miller and S. Flynn. *Gene* **308**: 67 (2003).

Kakar, S.S, H. Jin, B. Hong, J.W. Eaton and K.A. Kang. Proceeding of the 2006 Annual Conference on the International Society of Oxygen Transport to Tissue, August 2006, Louisville, KY (Accepted).

Kang, K.A. and B. Hong, Critical Reviews™ in *Eukaryotic Gene Expression* **16**(1): 45 (2006).

Kaul, Z., T. Yaguchi, S.C. Kaul, T. Hirano, R. Wadhwa and K. Taira. *Cell. Res.* **13**: 503 (2003).

Kawai, N., A. Ito, Y. Nakahara, M. Futakuchi, T. Shirai, H. Honda, T. Kobayashi and K. Kohri. *The Prostate* **64**: 373 (2005).

Kim, S., Y.T. Lim, E.G. Soltesz, A.M. De Grand, J. Lee, A. Nakayama, J.A. Parker, T. Mihaljevic, R.G. Laurence, D.M. Dor, L.H. Cohn, M.G. Bawendi and J.V. Frangioni. *Nat. Biotechnol.* **22**: 93 (2004).

Larson D.R., W.R. Zipfel, R.M. Williams, S.W. Clark, M.P. Bruchez, F.W. Wise and W.W. Webb. *Science* **300**: 1434 (2003).

Lawson, W.D., F.A. Smith and A.S. Young. *J. Electrochem. Soci.* **107**: 206 (1960).

Lermo, A., S. Campoy, J. Barbé, S. Hernández, S. Alegret and M.I. Pividori. *Biosens. Bioelectro.* **22**(9 – 10): 2010 (2007).

Leuschner, C., C. Kumar, M.O. Urbina, J. Zhou, W. Soboyejo, W. Hansel and F. Hormes. Nanotech. Technical Proceedings for the 2005 NSTI Nanotechnolgy Conference and Trade Show, **1**: 5 (2005).

Licha, K., R. Riefke, V. Ntziachristos, A. Becker, B. Chance and W. Semmler. *Photochem. Photobiol.* **72**: 392 (2000).

Loo, C., A. Lin, L. Hirsch, M.H. Lee, J. Barton, N. Halas, J. West and R. Drezek. *Technology in Cancer Research and Treatment* **3**: 33 (2004).

Loo, C., A. Lowery, N. Halas, J. West and R. Drezek. *Nano Lett*. **5**: 709 (2005).

Majoros, J.J., T.P. Thomas, C.B. Mehta and J.R. Baker, Jr. *J. Med. Chem.* **48**(19): 5892 (2005).

Matsuoka, F., M. Shinkai, H. Honda, T. Kubo, T. Sugita and T. Kobayasi. *Biomagn. Res. Technol.* **2**(1): 3 (2004).

Meyer, H.F.M., M. Hartmann, H.-J. Krause, G. Blankenstein, B. Mueller-Chorus, J. Oster, P. Miethe and M. Keusgen, Biosensors and Bioelectronics **22**: 973, (2007a).

Meyer, H.F.M., H.-J. Krause, M. Hartmann, P. Miethe, J. Oster and M. Keusgen, Journal of Magnetism and Magnetic Materials, **68**(2): 218, (2007b).

Meyer, H.F.M., M. Stehr, S. Bhuju, H.-J. Krause, M. Hartmann, P. Miethe, M. Singh and M. Keusgen, Journal of Microbiological Methods, **311**(1): 259, (2007c).

Mornet, S., S. Vasseur, F. Grasset and E. Duguet. *J. Mater. Chem.* **14**: 2161(2004).

Reddy, G.R., M.S. Bhojani, P. McConville, J. Moody, B.A. Moffat, D.A., Haoo, G. Kim, Y-E L., Koo, M.J., Wooliscroft, J.V. Sugai, T.D., Johnson, M.A. Philbert, R. Kopelman, A. Rehemtulla and B.D. Ross. *Clin. Cancer Res.* **12**(22): 6677 (2006).

Ruppin R. *Phys Rev* B. **11**(8): 2871 (1975).

Saito, R., J.R. Bringas, T.R. McKnight, M.F. Wendland, C. Mamot, D.C. Drummond, D.B. Kirpotin, J.W., Park, M.S., Berger and K.S. Bankiewicz. *Cancer Res.* **64**(7): 2573 (2004).

Sinha, R., G.J. Kim, S. Nie and D.M. Shin. *Mol. Cancer Ther.* **5**(8): 1909 (2006).

Shinkai, M., L. Biao, H. Honda, K. Yoshikawa, K. Shimizu, S. Saga, T. Wakabayashi, J. Yoshida and T. Kobayashi. *Cancer Science* **92**(10): 1138 (2001).

Shultz, M.D, S. Calvin, P.P. Fatouros, S.A. Morrison and E.E. Carpenter. *J. Magn. Magn. Mater.* **311**(1): 464 (2007).

Smith, AM, S. Dave, S. Nie, L. True and X. Gao. *Expert Rev Mol Diagn.* **6**(2): 231 (2006).

Soltesz E.G., S. Kim, R.G. Laurence, A.M. DeGrand, C.P. Parungo, D.M. Dor, L.H. Cohn, M.G. Bawendi, J.V. Frangioni and T. Mihaljevic. *Ann. Thorac. Surg.* **79**(1): 269 (2005).

Storm, F.K. *Hyperthermia in Cancer Therapy*. Boston: G. K. Hall Medical Publishers (1983).

Stroh, M., J.P. Zimmer, D.G. Duda, T.S. Levchenko, K.S. Cohen, E.B. Brown, D.T. Scadden, V.P. Torchilin, M.G. Bawendi, D. Fukumura and R.K. Jain. *Nat. Med.* **11**: 678 (2005).

Tanaka, K., A. Ito, T. Kobayashi, T. Kawamura, S. Shimada, K. Matsumoto, T. Saida and H. Honda. *J. BioSci. Bioengr.* **100**(1): 112 (2005).

Tartaj, P., M.P. Morales, S. Veintemillas-Verdaguer, T. Gonźalez-Carreno and C.J. Serna. *J. Phys. D: Appl. Phys.* **36**: R182 (2003).

Torchilin, V.P., European. *J. Pharma. Sci.* **11**(Supplement 2): S81 (2000).

Varshney M. and Li, Y. *Biosensors and Bioelectronics*, **22**(11): 2408 (2007).

Weissleder R., G. Elizondo, J. Wittenberg, C.A. Babito, H.H. Bengele and L. Josephson. *Radiol.* **175**: 489 (1990).

Yan, S., D. Zhang, N. Gu, J. Zheng, A. Ding and Z. Wang. *J. Nanosci. Nanotechnol.* **5**(5): 1185 (2005).

Yanase, M., M. Shinkai, H. Honda, T. Wakabayashi, J. Yoshida and T. Kobayshi. *Jpn. J. Cancer Res.* **89**: 463 (1998).

Yang, C., J. Xing, Y. Guan and H. Liu. *Appl. Microbiolo and Biotechnol.* **72**(3): 616 (2006).

Zhang, L.Y., H.C. Gu and X.M. Wang. *J. Magn. Magn. Mater.* **311**: 228 (2007).

Zhao, A.J., P. Yao, C.S. Kang, X. Yuan, J. Chang and P. Pu. *J. Magn. Magn. Mater.* **295**(1): 37 (2005).